University of Glasgow

Abánades Lázaro, I., Haddad, S., Rodrigo-Muñoz, J., Marshall, R. J., Sastre, B., del Pozo, V., Fairen-Jimenez, D. and Forgan, R. S. (2018) Surface-functionalisation of Zr-Fumarate MOF for selective cytotoxicity and immune system compatibility in nanoscale drug delivery. *ACS Applied Materials and Interfaces*, 10(37), pp. 31146-31157. (doi:10.1021/acsami.8b11652)

This is the author's final accepted version.

There may be differences between this version and the published version. You are advised to consult the publisher's version if you wish to cite from it.

http://eprints.gla.ac.uk/167570/

Deposited on: 24 August 2018

Enlighten – Research publications by members of the University of Glasgow
http://eprints.gla.ac.uk

Surface-Functionalisation of Zr-Fumarate MOF for Selective Cytotoxicity and Immune System Compatibility in Nanoscale Drug Delivery

Isabel Abánades Lázaro,[a] Salame Haddad,[b] Jose M. Rodrigo-Muñoz,[c] Ross J. Marshall,[a] Beatriz Sastre,[c] Victoria del Pozo,[c]* David Fairen-Jimenez[b]* and Ross S. Forgan[a]*

[a]WestCHEM School of Chemistry, University of Glasgow, Joseph Black Building, University Avenue, Glasgow G12 8QQ, UK.

E-mail: ross.forgan@glasgow.ac.uk; Web: www.forganlab.com

[b]Adsorption & Advanced Materials Laboratory, Department of Chemical Engineering & Biotechnology, University of Cambridge, Philippa Fawcett Drive, Cambridge CB3 0AS, UK.

E-mail: df334@cambridge.ac.uk

[c]Department of Immunology, Instituto de Investigación Sanitaria Fundación Jiménez Díaz, Universidad Autónoma de Madrid (IIS-FJD, UAM), and CIBER de Enfermedades Respiratorias (CIBERES), 28029 Madrid, Spain.

E-mail: VPozo@fjd.es

Keywords: metal−organic frameworks, drug delivery, surface modification, coordination modulation, endocytosis pathways, immune system response, dichloroacetate.

Abstract

Metal-organic frameworks (MOFs), network structures wherein metal ions or clusters link organic ligands into porous materials, are being actively researched as nanoscale drug delivery devices (DDSs) as they offer tuneable structures with high cargo loading that can easily be further functionalized for targeting and enhanced physiological stability. The excellent biocompatibility of Zr has meant that its MOFs are amongst the most studied to date, in particular the archetypal Zr terephthalate UiO-66. In contrast, the isoreticular analogue linked by fumarate (Zr-fum) has received little attention, despite the endogenous linker being part of the Krebs cycle. Herein, we report a comprehensive study of Zr-fum in the context of drug delivery. Reducing particle size is shown to increase uptake by cancer cells while reducing internalisation by macrophages, immune system cells that remove foreign objects from the bloodstream. Zr-fum is compatible with defect-loading of the drug dichloroacetate, as well as surface modification during synthesis, through coordination modulation, and postsynthetically. DCA-loaded, PEGylated Zr-fum shows selective *in vitro* cytotoxicity towards HeLa and MCF-7 cancer cells, likely as a consequence of its enhanced caveolae-mediated endocytosis compared to uncoated precursors, and it is well tolerated by HEK293 kidney cells, J774 macrophages, and human peripheral blood lymphocytes. Compared to UiO-66, Zr-fum is more efficient at transporting the drug mimic calcein into HeLa cells, and DCA-loaded, PEGylated Zr-fum is more effective at reducing HeLa and MCF-7 cell proliferation than the analogous UiO-66 sample. *In vitro* examination of immune system response shows Zr-fum samples induce less reactive oxygen species than UiO-66 analogues, possibly as a consequence of the linker being endogenous, and do not activate the C3 and C4 complement cascade pathways, suggesting that Zr-fum can avoid phagocytic activation. The results show that Zr-fum is an attractive alternative to UiO-66 for nanoscale drug delivery, and that a wide range of *in vitro* experiments are available to greatly inform the design of DDSs prior to early stage animal studies.

Introduction

The requirement for new cancer treatments is driven by increases in the diagnosed cases of cancer, the side effects of most available therapeutics, and the resistance of some tumours towards them.[1-3] Interest in drug delivery systems (DDSs) is increasing, with the ultimate aim of selectively targeting cancer cells with nanoscale "Trojan horses" capable of delivering therapeutic cargo directly to sites of disease.[4-5] However, clinical application of DDSs faces drawbacks such as poor drug loading capacity,[6] fast drug release kinetics,[7] aggregation in the bloodstream,[8] non-specific biodistribution or accumulation in the body[9] and, in some cases, toxicity.[10] Developing model DDSs and methodology for their surface modifications, with the aims of controlling their physical properties and understanding the correlation between the former and their therapeutic activity, is of vital importance to ultimately lead to the design of novel DDSs.[11] Among these drug delivery devices, metal-organic frameworks (MOFs)[12-13] – a new generation of highly porous, crystalline structures comprised of organic and inorganic components – have emerged as an alternative to combine the most attractive properties of organic (biocompatibility, targeted bio-distribution)[14-15] and inorganic (high drug loadings, biostability)[16-17] DDSs, making MOFs highly promising candidates to overcome the problems that nanomedicine is currently facing.[18-20]

Zirconium-based MOFs have recently acquired significant interest as potential DDSs, as they are generally more thermally, mechanically and chemically stable than other MOF systems but will still degrade slowly under physiological conditions,[21-22] while at the same time Zr has good biocompatibility[23] and they are amenable to postsynthetic modification.[24] For example, the Zr terephthalate MOF UiO-66,[25] where UiO stands for University of Oslo, and other MOFs of the UiO isoreticular series with ideal formula $[Zr_6O_4(OH)_4L_6]_n$,[26] have been postsynthetically modified with a number of surface moieties, including poly-*N*-isopropylacrylamide (PNIPAM),[27-28] poly(ethylene glycol) (PEG),[29] DNA sequences,[30-31] small interfering RNA (siRNA),[32] phospholipid bilayers,[33] L-dopamine,[34] and anticancer targeting units[35] among others. Surface coatings have been proven to improve simulated physiological stability, colloidal dispersion and drug release kinetics, among other properties.

While UiO-66 and the more porous MOFs of the UiO-66 series of MOFs have received widespread attention as potential DDSs,[26, 36] application of the isoreticular MOF composed of the endogenous fumarate linker are rare.[37] So-called Zr-fum (Figure 1) has a similar structure to UiO-66, but its porosity is reduced compared to the rest of the series (S_{BET} ~800 m^2g^{-1}) as the fumarate linker, an intermediate of the Krebs cycle, is shorter in length.[38] Zr-fum can be synthesised in water,[38-39] and has requisite stability for application in water adsorption[40] and harvesting,[41] catalysis,[42] and aqueous fluoride sequestration.[43]

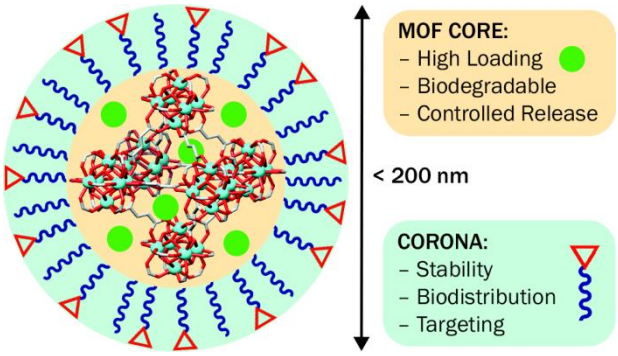

Figure 1. Schematic showing the Zr-fum structure with preferred properties of a MOF-based drug delivery device.

The potential application of Zr-fum nanoparticles of 83 ± 14 nm size as a DDS has been studied by Lachet and co-workers,[37] by coordinating various pro-apoptotic peptides and a cytochrome c protein (CytC) to the external surface of the MOF using the imidazole groups of terminal oligohistidine residues (His-tags). The coating was proven to be stable at pH 7.4 in HEPES buffered glucose (HBG), while partially released at pH 5, and completely cleaved at pH 3. Between 20 and 30 fold-increases in the internalisation of the various peptides by HeLa cervical cancer cells when attached to Zr-fum were observed; increases in cytotoxicity towards HeLa cells occur when pro-apoptotic peptides are delivered by the MOF, whereas free peptides are not cytotoxic as they cannot efficiently enter the cell. Additionally, the dye resorufin has been postsynthetically encapsulated in Zr-fum nanoparticles, followed by coating with galactosylamine, and used for intracellular imaging with no appreciable *in vitro* cytotoxicity towards FL83B and HepG2 cells.[44] These promising results demonstrate the requirement for a systematic study into the functionalization, stability, degradation, and cytotoxicity of Zr-fum to assess its general performance as a DDS *in vitro*.

The coordination modulation process,[45] in which monodentate ligands (modulators) are introduced to MOF syntheses and compete with the multidentate linkers for the metal coordination sites, has been widely used to control the particle size of MOFs[46-47] and to enhance their physical properties, such as crystallinity and porosity.[48] The addition of modulators to synthesis of Zr MOFs is known to induce defects, such as missing clusters and linkers, and also install functionality on particle outer surfaces.[28, 49-50] This process has been widely studied for UiO-66, and modulator incorporation has been found to be pK_a dependent.[51] While modulation is known to control the particle size of Zr-fum,[38-39] the MOF has not received special attention for defect engineering.

We have recently exploited this phenomenon to load an anticancer metabolic target, dichloroacetic acid (DCA), at defect sites within the bulk of Zr MOFs of the UiO-66 family during synthesis.[49] These defects enhance their porosity, which can be used to store a

second anticancer drug, 5-fluorouracil (5-FU), resulting in dual drug loaded MOFs. The low pK_a of DCA, together with its small size, ensures high incorporation (ca. 20% *w/w*) even in the presence of other modulators.[28-29] Incorporation of both the cancer targeting folic acid (FA), and functionalised modulators, such as *p*-azidomethylbenzoic acid (L1), which can be further transformed by click chemistry, allow the assembly of surface functionalised, drug loaded UiO-66 nanoparticles which exhibit selective anticancer cytotoxicity.

Herein, we extend these surface functionalization protocols to Zr-fum, aiming to develop protocols for the control of (i) particle size, in order to study the size dependence of Zr fumarate on its physical properties (i.e. colloidal dispersion and phosphate stability) and on its cellular uptake by cancer cells and macrophages, and (ii) surface chemistry, to find any correlation with physical properties and *in vitro* performance, with the ultimate aim of assessing the potential for *in vivo* application of Zr-fum.

Results and discussion

Particle Size Control. The cellular internalisation pathways by which nanoparticulate DDSs are internalised are size dependent.[52-55] Nano-devices are often internalised by eukaryotic cells through active transport such as endocytosis, although if small enough (<20 nm) DDSs can be internalised by passive diffusion. Among endocytosis pathways, the most studied are receptor-mediated endocytosis (i.e. caveolae or clathrin-mediated),[55] non-mediated endocytosis, and macropinocytosis.[56] It has been reported that DDSs internalised through the caveolae-mediated route could be more successful in delivering their cargo into the cytosol, due to endosomal escape through DDS encapsulation in caveosomes.[57] Macrophages, the cells responsible for removing foreign bodies from the blood current, usually internalise matter through phagocytosis.[58]

To study how size affects the internalisation of Zr-fum by cancer cells and macrophages, crystalline (Figure 2a) nanoparticles of different sizes were synthesised utilising two different metal precursors, $ZrCl_4$ and $ZrOCl_2 \cdot 8H_2O$, with acetic acid as a modulator (See SI, Section S2). The large sample, Zr-fum (b), where b stands for big, is 168 ± 24 nm in diameter, as determined by SEM (Figure 2b), while Zr-fum (s), where s stands for small, is 23 ± 11 nm in size (Figure 2c), explaining the broadening of reflections in its powder X-ray diffraction (PXRD) pattern. Full characterisation (SI, Section S4.1) – including FTIR spectroscopy, thermogravimetric analysis (TGA) and N_2 adsorption and desorption isotherms – confirmed the samples to be thermally stable and porous (S_{BET} = 865 m^2g^{-1} and 596 m^2g^{-1} for Zr-fum (s) and Zr-fum (b) respectively). The pore volume of Zr-fum (s) at 0.98 p/p_0 (0.978 cm^3g^{-1}) compared to Zr-fum (b) (0.364 cm^3g^{-1}) suggests a high degree of defectivity, although it is possible this is filling of interparticle space between the very small nanoparticles.

Dynamic light scattering (DLS) measurements were performed in water (Figure 2d). Zr-fum (s) displays aggregates of size approximately 75 nm, while Zr-fum (b) forms aggregates of around 300 nm. This small amount of aggregation is in good agreement with the previous report from Lachelt and co-workers,[37] where nanoparticles of 83 ± 14 nm (SEM) showed aggregation in DLS measurements to 132 nm (ethanol) and 182 nm (water).

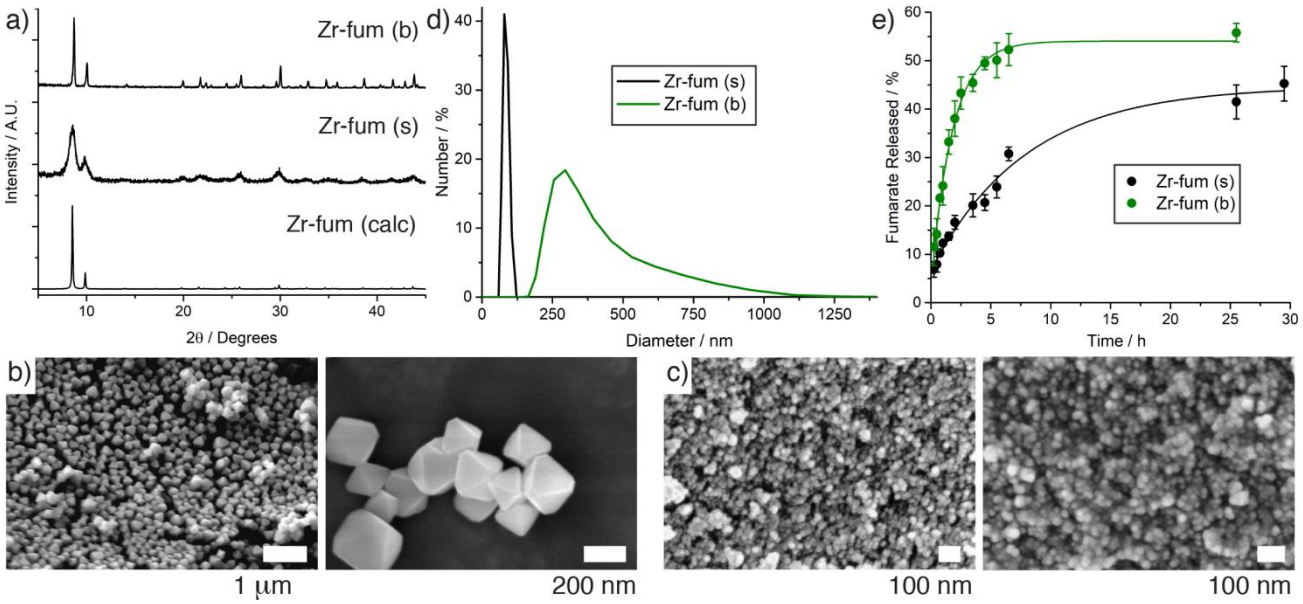

Figure 2. a) Stacked PXRD patterns for the Zr-fum samples compared to that calculated from its single crystal structure (CCDC ref code BOHJOZ).[40] SEM images of b) Zr-fum (b) and c) Zr-fum (s) at different magnifications. d) Particle size distributions of the samples dispersed in water as measured by DLS. e) Degradation profiles in PBS 10X (pH 7.4) for the two samples as measured by UV/Vis spectroscopic determination of fumarate release.

The stability of the samples in PBS 10X (pH = 7.4) was investigated through UV-Vis spectroscopic determination of fumarate release, showing the smaller sample to be initially more stable, but reaching similar levels of linker release after 24 h (Figure 2e). While Zr-fum (b) degrades with an exponential profile, reaching a plateau of 58% linker release after 8 h, the smaller analogue degrades with a two-step profile, with a slower rate during the first 3 h (releasing 20% vs 45% for the bigger analogue). Interestingly, Zr-fum seems to be more stable towards phosphate-induced degradation than UiO-66, which releases ~80% of its linker after a few hours.[28] This is possibly a consequence of the lower pK_a of fumaric acid compared to terephthalic acid resulting in a more stable metal-carboxylate bond, and thus enhancing the competition between free phosphates and carboxylates for the coordination to the Zr clusters.

To monitor cellular uptake, a carboxylate containing fluorescent molecule, calcein, was postsynthetically loaded into the samples. Calcein is not able to efficiently cross the cell

membrane due to its hydrophilicity (logP = -4),[59] and so it is an excellent probe for the cellular internalisation of MOFs.[60] Calcein loading in cal@Zr-fum (s) was considerably higher (16.8% *w/w*) than for cal@Zr-fum (b) (3.4% *w/w*), presumably as a consequence of thes higher degree of defects and greater external surface-to-bulk ratio of the former compared to the latter. It has been previously reported for UiO-66 that, due to the size of calcein, the molecule is not able to efficiently penetrate the porosity of the MOF, and so it is most likely to be coordinated to Zr clusters at the outer surface and at defect sites through its carboxylate groups.[29] Zr-fum has a smaller pore window than UiO-66;[25, 38] TGA and FTIR measurements confirm that external surface loading also occurs for Zr-fum (SI, Section S4.2.).

Fluorescence assisted cell sorting (FACS) was used to monitor the cellular internalisation of the cal@MOFs (SI, Section S3), showing that the smaller cal@Zr-fum (s) was more efficiently internalised by HeLa cervical cancer cells (by a factor of 2.3), while cal@Zr-fum (b) was better internalised by J774 macrophages (by a factor of 1.6) (Figure 3a). Importantly, cal@Zr-fum (s) was able to deliver calcein into HeLa cells with a 20-fold increase compared to free calcein, which is considerably higher than previously found for cal@UiO-66 (5-10 fold increase).[28, 61] The use of inhibitors of certain endocytic pathways[28] – chlorpromazine and sucrose for clathrin-mediated endocytosis (although sucrose also inhibits non-mediated pathways), nystatin for caveolae-mediated endocytosis, and rottlerin for macropinocytosis – enables an assessment of the effect of particle size on the major routes of internalisation of Zr-fum by HeLa cancer cells when compared to uninhibited cellular uptake (Figure 3b). Lachet's previous study of internalisation routes involved Zr-fum nanoparticles[37] (surface modified with a fluorescent peptide) of size ~ 83 nm, an intermediate size compared to the MOFs here presented (~25 nm and ~170 nm). The surface modified MOF was partially internalised through the caveolae-mediated route, with minor contribution of macropinocytosis. Zr-fum (b) was internalised primarily through macropinocytosis (~44 ± 5% inhibition by rottlerin), showing only a minor contribution of clathrin-mediated endocytosis. This pathway plays a more important role in the internalisation of Zr-fum (s) (~31 ± 2% inhibition by chlorpromazine), whereas macropinocytosis does not play a significant role for the smaller MOF. Inhibition of the caveolae-mediated pathway does not alter the cellular internalisation of either of the MOFs, indicating that uptake by HeLa cells does not occur through the caveolae-mediated pathway. It is likely the caveolae-mediated uptake observed by Lachet[37] is induced by the peptides attached to the surfaces of their Zr-fum sample, and we have observed a similar effect when coating UiO-66 with poly(ethylene glycol) (PEG) chains.[29]

To assess the contribution of non-active transport (i.e. passive diffusion) a control in which the cells were incubated with the MOFs at 4 ºC, a temperature at which most cellular

functions are attenuated,[62] was performed and normalised to the cellular internalisation at 37 ºC (Figure 3b). The higher degree of internalisation of cal@Zr-fum (s) at 4 ºC (37 ± 1% vs 21 ± 1% for cal@Zr-fum (b)) indicates that passive diffusion could play some role in its cellular internalisation, although not to the same extent as active transport, which is of greater importance. Passive diffusion can also facilitate cytosolic localisation, which is favourable for drug delivery.[63]

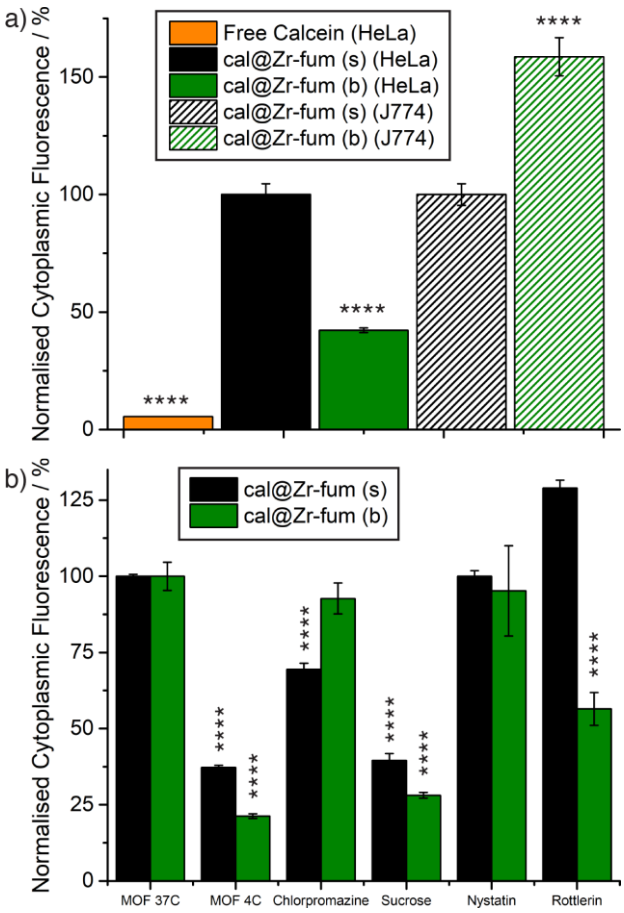

Figure 3. a) Endocytosis efficiencies of cal@Zr-fum (s) and cal@Zr-fum (b) towards HeLa and J774 cells, compared to free calcein, and normalised to the values for cal@Zr-fum (s). b) Endocytosis efficiencies of the two samples towards HeLa cells in the presence of inhibitors for certain endocytic pathways. The statistical significance compared to the control was determined by ordinary one-way ANOVA and is indicated on the graph: *P<0.05; **P<0.01 ***P < 0.001 and ****P < 0.0001.

Surface Functionalisation. Due to these encouraging results – particle size reduction resulting in an enhancement in internalisation cancer cells internalisation, with possible passive diffusion, and a decrease in macrophage recognition – cal@Zr-fum (s) was selected for further study. Surface modifications with folic acid (targeting)[64] and PEG (dispersion, immune system avoidance)[65] were attempted during synthesis and postsynthetically (Scheme 1), following our previously reported protocols (SI, Section S2).[28-29] To maintain particle size, the surface of Zr-fum (s) was addressed with p-azidomethyl benzoic acid (L1)

and folic acid (FA) postsynthetically, using the surface ligand exchange (SLE) protocol, to yield Zr-fum-L1 (s) and Zr-fum-FA (PS), respectively, where PS stands for postsynthetic. The azide functionality of L1 was subsequently used to covalently attach propargyl-terminated PEG2000 chains to the outer surface of the MOF through copper-catalysed azide-alkyne cycloaddition (CuAAC), to form Zr-fum-L1-PEG2000 (s). Additionally, Zr-fum-FA (CM) was prepared through co-modulation with folic acid and acetic acid, where CM stands for coordination modulation, in order to study the effect of coating protocol on the colloidal dispersion and stability towards phosphate attack.

Scheme 1. Synthetic scheme for the synthesis of surface-functionalised Zr-fum samples.

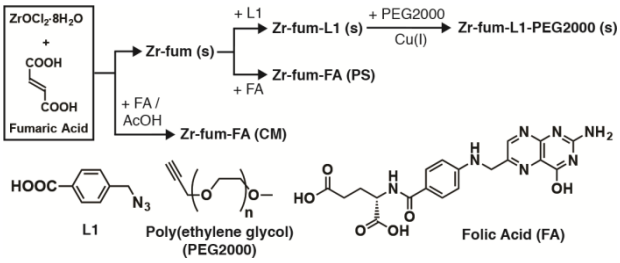

Full characterisation of the samples (SI, Section S5) confirms the incorporation of the surface functionalities, with retention of crystallinity confirmed by PXRD. ^{1}H NMR spectra of acid digested samples contain characteristic resonances for protons of L1 and folic acid, with a content of ca. 19 mol % and 17 mol %, both compared to fumarate, for L1 and folate, respectively. The azide functionality of L1 was identified in the FT-IR spectrum of Zr-fum-L1 (s), while the carboxylate band of folic acid is shifted in the FT-IR spectra of both Zr-fum-FA (PS) and Zr-fum-FA (CM) as a consequence of folate attachment to the available Zr clusters. Vibration bands characteristic of the PEG moieties are also observed in the FT-IR spectrum of Zr-fum-L1-PEG2000 (s), while disappearance of the azide band is a consequence of the CuAAC reaction and consequent covalent attachment. TGA profiles showed similar features to those of previously reported analogous UiO-66 samples;[28-29] a decrease in residual ZrO_2 content of all samples, more gradual decomposition profiles for the folate-coated samples, and earlier structure decomposition upon PEGylation. A decrease in porosity was also observed for the postsynthetically coated samples (S_{BET} = 504 m^2g^{-1}, 628 m^2g^{-1}, and 570 m^2g^{-1} for Zr-fum-FA (PS), Zr-fum-L1 (s), and Zr-fum-L1-PEG2000 (s), in turn) in great agreement with surface reagent incorporation, whereas Zr-fum-FA (CM) was highly porous (S_{BET} = 821 m^2g^{-1}) as a consequence of the induction of defects through folate attachment during synthesis.

Although the aggregation of Zr-fum (s) in water was not remarkable (~75 nm), its colloidal stability was slightly improved upon PEGylation (~70 nm), and to a higher extent upon folate coating (~50 nm) (Figure 4a). The sample prepared through coordination modulation, Zr-

fum-FA (CM), displayed aggregates of ~250 nm, close to the size determined by SEM (~170 nm). The degradation of the samples was measured in PBS 10X (pH 7.4) (Figure 4b). An induction period, more pronounced than for the precursor Zr-fum (s), was observed upon PEGylation, in which Zr-fum-L1-PEG2000 (s) only releases <5% of the fumarate linker during the first hour, although subsequently degrading with a similar profile, within error, to its precursor after 1.5 h, possibly as a consequence of detachment of the PEG corona. In contrast, Zr-fum-FA (PS) degraded faster than its precursor, whereas the folate-modulated sample Zr-fum-FA (CM) was remarkably more stable than the bare MOF, with an induction time similar to the postsynthetically PEGylated sample and a slower degradation rate, reaching a plateau of 20% linker release after 6 h of degradation and not releasing any further linker after 25 h. These results indicate that the nature of the coating plays an important role during the samples degradation.

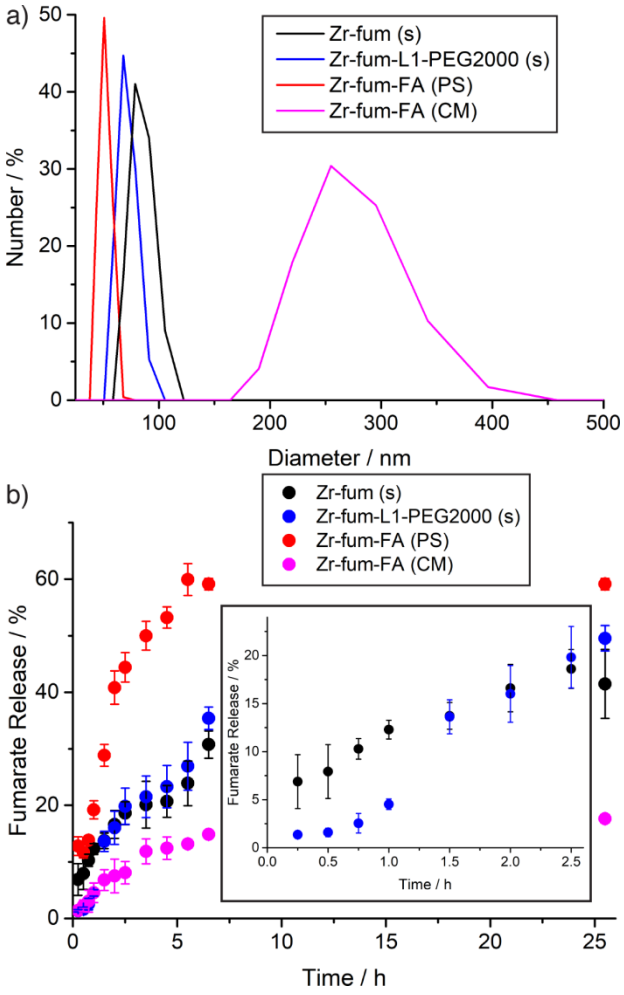

Figure 4. a) Particle size distributions of the Zr-fum samples in water measured by DLS. b) Degradation profiles in PBS 10X (pH 7.4) of the Zr-fum samples measured by UV/Vis determination of fumarate release, with the inset showing the induction period of prolonged stability for the PEGylated sample compared to the uncoated one.

In order to study the effect of surface coating on cellular internalisation of the MOFs, calcein was loaded into Zr-fum (s) and Zr-fum-L1 (s), to yield cal@Zr-fum (s) and cal@Zr-fum-L1 (s), respectively (Scheme 2). The former was postsynthetically coordinatively coated with folic acid, while the latter was PEGylated covalently by CuAAC, using the same postsynthetic modification protocols as previously. Full characterisation (SI Section S5.2) confirmed the attachment of the surface reagents to the surface of cal@Zr-fum (s).

Scheme 2. Synthetic methodology for preparing calcein loaded Zr-fum samples.

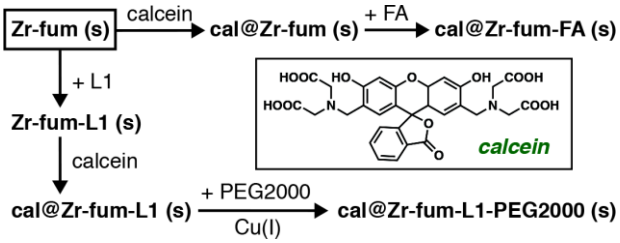

The efficacy of internalisation of the MOFs by HeLa and J774 macrophage cells was assessed by FACS (Figure 5a). Coating the surface of Zr-fum (s) with L1 did not significantly alter HeLa internalisation, whereas PEGylation decreased cell internalisation by 42 ± 2%, possibly as a consequence of the more neutral surface. Folate coating increased the MOF internalisation by 58 ± 5% compared to the bare MOF, possibly as a consequence of the overexpression of folate receptors on the surface of HeLa cervical cancer cells.[66] J774 macrophage internalisation was also investigated, showing a slight increase in uptake upon PEGylation (134 ± 12%) and a non-significant increase after folate coating (114 ± 12%) compared to the non-coated sample cal@Zr-fum (s) (100 ± 5%). Of all the samples studied, cal@Zr-fum (b) was still the most internalised MOF by macrophages, with 159 ± 8% internalisation compared to cal@Zr-fum (s) (Figure 3).

Analysis of HeLa cell endocytosis routes of the samples was also performed. Incubation at 4 ºC decreased cell internalisation of cal@Zr-fum-L1 (compared to incubation at 37 °C) to similar levels as its precursor cal@Zr-fum (s) (33 ± 3% uptake *vs* 37 ± 1%), whereas the effect was less pronounced for the PEGylated (62 ± 4% uptake) and folate-coated MOFs (79 ± 5% uptake), indicating a higher contribution of non-active transport (Figure 5b). It is important to consider that although the average particle size distribution of Zr-fum (s) (23 ± 11 nm) is slightly above the size expected to allow passive diffusion through the cell membrane, a considerable portion of the nanoparticles is smaller than 20 nm (Figure S5), and so, after surface coating with more lipophilic moieties, the passive diffusion of this population of smaller nanoparticles could be enhanced.[67]

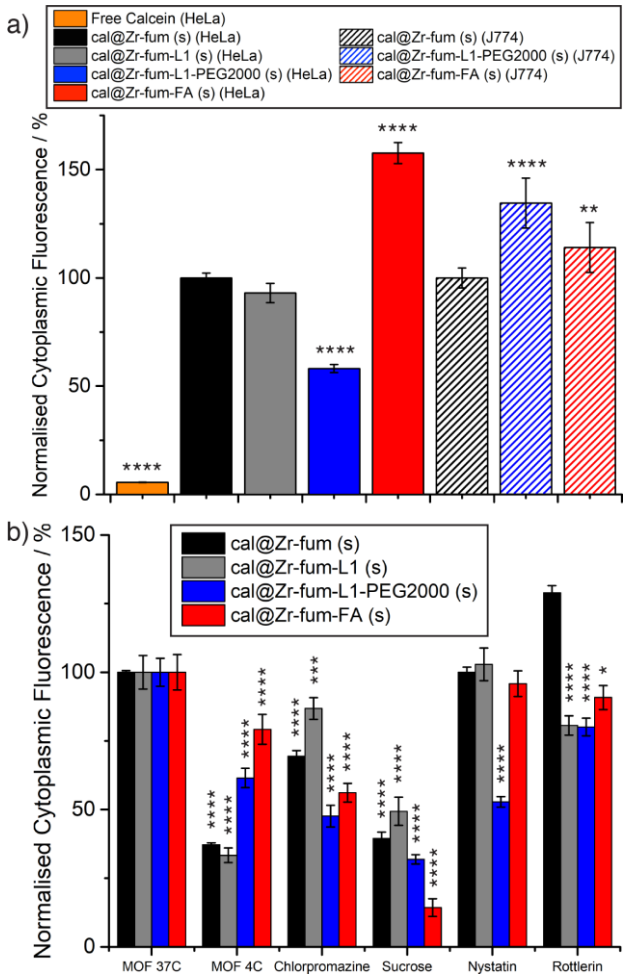

Figure 5. a) Endocytosis efficiencies of the surface-modified Zr-fum samples towards HeLa and J774 cells, compared to free calcein, and normalised to the values for cal@Zr-fum (s) for each cell line. b) Endocytosis efficiencies of the samples towards HeLa cells in the presence of inhibitors for certain endocytic pathways. The statistical significance compared to controls was determined by ordinary one-way ANOVA and is indicated on the graph: *P<0.05; **P<0.01 ***P < 0.001 and ****P < 0.0001.

The high degree of inhibition upon incubation with sucrose for all MOFs indicates non-mediated transport contributes to their internalisation. Apart from a small decrease in the contribution of macropinocytosis and clathrin-mediated endocytosis, the routes of internalisation of cal@Zr-fum-L1 (s) did not vary significantly compared to the bare analogue (Figure 5b). Higher degrees of clathrin-mediated endocytosis participation were observed after surface modifications with folate and PEG, for which inhibition of 48 ± 3% and 52 ± 4% were respectively observed after incubation with chlorpromazine. A decrease in internalisation of cal@zr-fum-L1-PEG2000 (s) (~48 ± 2%) upon incubation with nystatin indicates significant contribution of the caveolae-mediated route, in good agreement with our previous work, where PEGylation induces caveolae-mediated HeLa cell uptake of cal@UiO-66 (~150 nm).[29] These results suggest that coating different MOFs with PEG chains can induce uptake through caveolae mediated-endocytosis, seemingly without a major size

effect. On the other hand, in contrast to cal@UiO-66-FA, which was determined to be partially internalised by caveolae-mediated endocytosis,[28] the internalisation of cal@Zr-fum-FA (s) was not inhibited by nystatin. This may be a consequence of passive diffusion still occurring in the presence of nystatin due to the small particle size, but this would also be expected to occur when the clathrin-mediated pathway is inhibited by chlorpromazine.

Drug Delivery. Dichloroacetate (DCA) is a pyruvate dehydrogenase kinase (PDK) inhibitor.[68] Thus, DCA shifts cancer cell metabolism from glycolysis back to glucose oxidation by pyruvate dehydrogenase re-activation, unlocking cancer cells from a state of apoptosis resistance without affecting growth of healthy cells.[69-70] However, the hydrophilic nature of DCA means it does not efficiently cross the cell membrane,[71] resulting in limited ability to reach its target and rapid clearance from the bloodstream.[72] Consequently, DCA has half maximum effective concentration (EC_{50}) values in the millimolar range,[73] meaning that doses three orders of magnitude higher than for current anticancer drugs are needed to induce a similar therapeutic effect. Nevertheless, *in vitro* studies have shown remarkably lower resistance factors towards DCA compared to other anticancer therapeutics,[73-74] and DCA has also been shown to enhance the anticancer effect of well-known drugs such as 5-fluorouracil and cisplatin.[73, 75-76] While DCA is not currently under clinical use as an anticancer drug, several clinical trials have shown that DCA treatment induces significant tumour remission with very low side effects and toxicity compared to other therapeutics.[77-80] DCA's excellent therapeutic activity combined with its poor cellular internalisation makes it a highly informative mechanistic probe to study the potential effect of MOFs as DDSs, as a substantially enhanced cytotoxicity will be a consequence of efficient internalisation of the MOFs and the subsequent release of their cargo into the cytosol.

In order to study the effect of particle size and surface chemistry on therapeutic activity, dichloroacetic acid was introduced as a modulator of Zr-fum synthesis, with or without the co-modulation of folic acid, to prepare DCA@Zr-fum (s) and DCA@Zr-fum-FA (CM), respectively (Scheme 3).

Scheme 3. Synthetic scheme for DCA-loaded, surface modified Zr-fum samples.

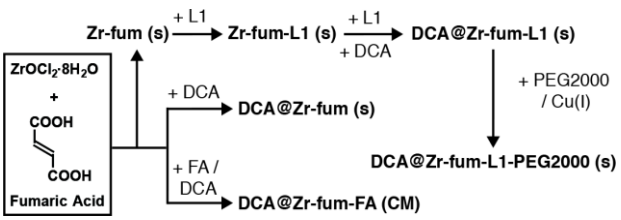

Figure 6 shows the typical analytical techniques used to monitor DCA incorporation into DCA@Zr-fum (s) (see SI Section S6 for full characterisation of other samples). DCA is an

effective modulator of Zr MOFs, with crystallinity retained but weak broad reflections indicating small particle size and/or defectivity (Figure 6a). As a consequence of the low pK_a of DCA (~1.4), its incorporation into the MOFs at defect sites was considerable (~20% *w/w*). Loading can be assessed by thermogravimetric analysis (TGA, Figure 6b) so long as its thermal decomposition does not overlap with surface functionality, and confirmed by ICP-MS analysis of Cl content (20.4% *w/w* for DCA@Zr-fum (s)). FT-IR spectra (Figure 6c) also showed its presence within the MOF samples, with a shifting of the DCA carbonyl stretch from ca. 1730 cm^{-1} to 1650 cm^{-1} indicating its coordination to the Zr clusters. The particle size distributions, determined by SEM (Figures S43-S46), highlight the role of the modulators during the crystallisation process. DCA@Zr-fum (s) has a homogenous size distribution profile composed of nanoparticles with an average size of 28 ± 9 nm, whereas the particle size increases noticeably for DCA@Zr-fum-FA (CM), with size distribution profiles of ca. 99 ± 19 nm, while both samples are relatively well dispersed in water, with average sizes of ~75 and ~ 250 nm, respectively. The folate content of DCA@Zr-fum-FA (CM) was determined by UV-Vis spectroscopy of digested samples and found to be significant (17.9% *w/w*) indicating incorporation in the bulk as well as at the outer surfaces. DCA loading could be measured by ICP-MS and was found to be 19.5% *w/w*. N_2 adsorption and desorption measurements proved the samples to be porous despite the high DCA and folate content, with S_{BET} = 622 m^2g^{-1} and 482 m^2g^{-1} for DCA@Zr-fum (s) and DCA@Zr-fum-FA (CM) respectively, with the lower porosity of the latter indicative of significant incorporation of folate.

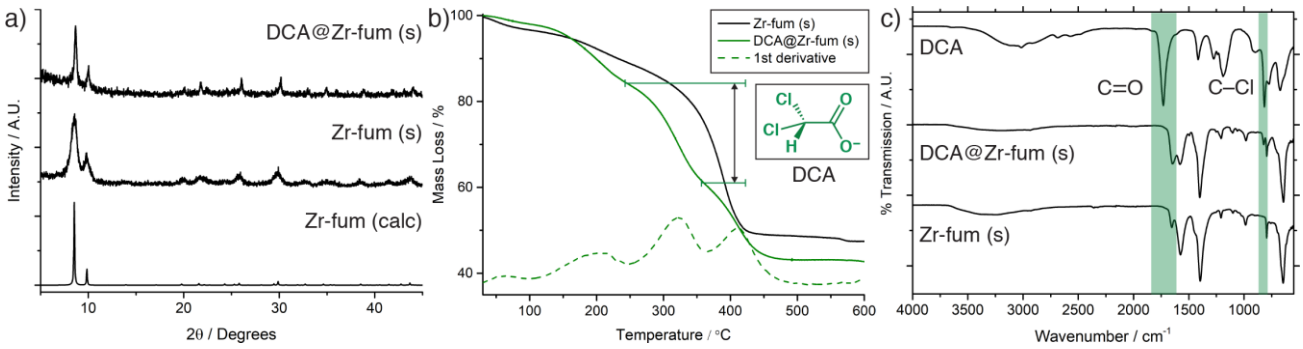

Figure 6. Comparison of DCA@Zr-fum (s) with Zr-fum (s). a) Partial stacked PXRD patterns showing retention of crystallinity on DCA loading. b) TGA traces showing DCA degradation around 250-350 °C. c) Stacked IR spectra showing the presence of DCA and the shifting of the carbonyl stretch of DCA when coordinated to Zr-fum.

Zr-fum-L1 (s) was postsynthetically loaded with DCA (Scheme 3) by stirring in a methanolic solution containing DCA (10% *v/v*) and L1 (1 $mgmL^{-1}$), to ensure that DCA attachment to the Zr positions will not result in the displacement of L1, as the pK_a of DCA is considerably lower than for benzoic acid derivatives. ^{1}H NMR spectra of acid-digested DCA@Zr-fum-L1 (s)

confirmed the presence of both L1 (~7 mol % compared to fumarate) and DCA (~40 mol %). DCA loading was also calculated by ICP-MS and TGA, with both techniques confirming approximately 20% *w/w* loading (ICP-MS: 21.1% *w/w*). The azide functionality of L1 was subsequently reacted with propargyl-terminated PEG2000 by CuAAC, leading to DCA@Zr-fum-L1-PEG2000 (s). The thermal decomposition of DCA and PEG occur at similar temperatures, resulting in an overall structure decomposition and hindering DCA determination by TGA in the PEGylated sample (Figure S53). The DCA loading of 12.1% *w/w*, determined by ICP-MS, is lower than the precursor – a consequence of the extra addition of mass through the PEG chains and possible detachment of some of the DCA under reaction conditions (acetic acid is used as a co-ligand for the Cu(I) catalyst). DLS showed the sample had a similar minor degree of aggregation in water to its precursor.

For comparison. the biocompatibility of the bare and surface-modified samples without cargo – Zr-fum (s), Zr-fum-FA (PS) and Zr-fum-L1-PEG2000 (s) was investigated by incubation with HeLa cervical cancer cells (Figure S60), showing >100% proliferation compared to controls after incubation with 1 $mgmL^{-1}$ of the MOFs for 72 h, as determined by the MTS assay. Increased proliferation could be a consequence of cellular metabolisation of the endogenous fumarate linker. Incubation of HeLa cancer cells (Figure 7a) with DCA@Zr-fum (s) and DCA@Zr-fum-FA (CM) for 72 h did not affect HeLa cell proliferation, whereas DCA@Zr-fum-L1-PEG2000 (s) was highly cytotoxic at concentrations of 0.5 $mgmL^{-1}$ after 24 h. The cytotoxicity of the PEGylated sample is possibly a consequence of its partial internalisation through caveolae-mediated endocytosis,[57] while it is significantly more cytotoxic towards HeLa than its UiO-66 analogue,[29] suggesting that Zr-fum is more effective at delivering DCA into the cells. It is important to take into account that although DCA@Zr-fum (s) has a particle size distribution (29 ± 9 nm) similar to Zr-fum (s) (23 ± 11 nm), the fraction of nanoparticles smaller than 20 nm is less significant, as can be observed in the particle size distribution histograms (Figure S46), meaning that passive diffusion may be less prevalent for this sample. DCA@Zr-fum-FA (CM) is bigger in size (ca. 100 nm), comparable to cal@Zr-fum (b), which was proven not to be internalised significantly by HeLa cells compared to the smaller analogues. Additionally, folate-coated cal@Zr-fum-FA (PS) did not show any significant caveolae-mediated uptake, which seems to be key to efficient DCA cytotoxicity. The PEGylated MOF has the lowest DCA loading (12.1% *w/w*), thus enhancing the therapeutic effect of the free drug by a factor of over 200[28] and highlighting the importance of the endocytosis routes of the DDSs on therapeutic efficacy.

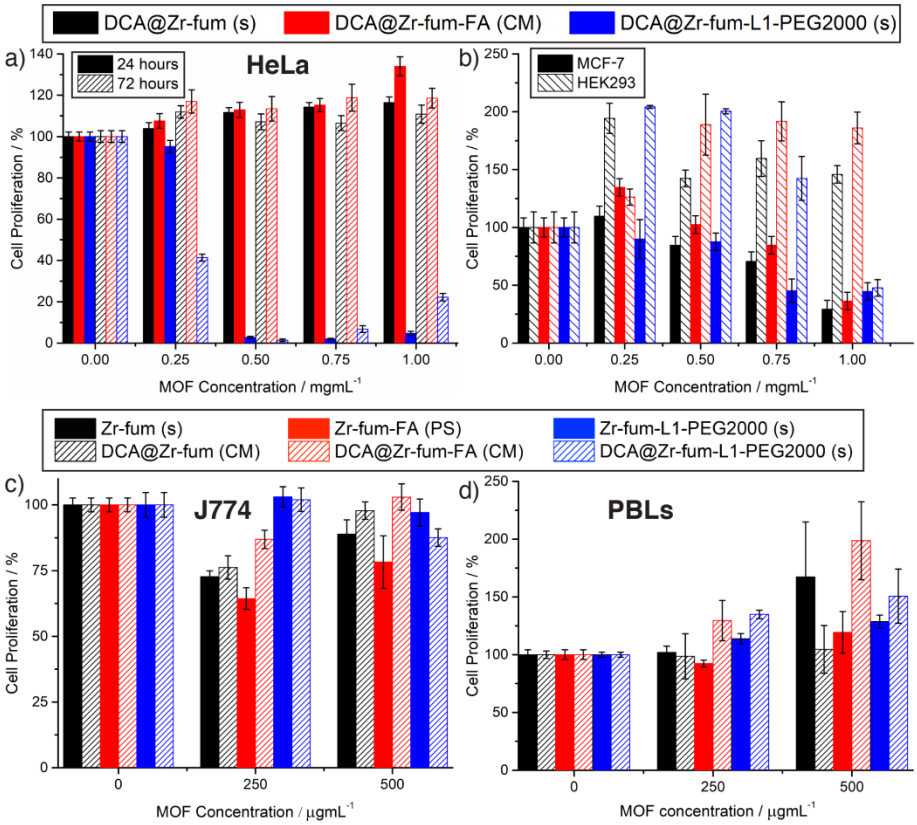

Figure 7. Cytotoxicity of DCA-loaded Zr-fum samples measured by MTS assay towards a) HeLa cells over 24 and 72 h incubation, and b) MCF-7 and HEK293 cells for 72 h. Cytotoxicity of empty and DCA-loaded Zr-fum samples measured by MTT assay towards c) J774 macrophage cells and d) peripheral blood lymphocytes isolated from human donors. Plots of cytotoxicity against DCA concentrations in the respective MOFs, with appropriate statistical analyses, are provided in the SI Section S7.

The selectivity of cytotoxicity was investigated against MCF-7 human breast carcinoma and HEK293 human embryonic kidney cell lines (Figure 7b). DCA@Zr-fum (s) and DCA@Zr-fum-FA (CM) have a moderate cytotoxic effect towards MCF-7 breast cancer cells (29 ± 8% and 36 ± 8% cell proliferation at 1 $mgmL^{-1}$, respectively), whereas both MOFs were non-cytotoxic towards HEK293 kidney cells (145 ± 8% and 186 ± 14% cell proliferation at 1 $mgmL^{-1}$, respectively). DCA@Zr-fum-L1-PEG2000 (s) has a similar cytotoxic effect towards MCF-7 cells (45 ± 10% and 44 ± 7% cell proliferation at 0.75 and 1 $mgmL^{-1}$, respectively), however, its non-selective cytotoxicity towards HEK293 at higher concentrations – 145 ± 43% cell proliferation at 0.75 $mgmL^{-1}$ decreases rapidly to 48 ± 7% proliferation at 1 $mgmL^{-1}$ – might indicate potential problems towards *in vivo* application if significant accumulation is observed. A similar effect has been seen previously for DCA delivery with analogous PEGylated UiO-66 at the same dosage,[28] and overall, DCA@Zr-fum-L1-PEG2000 (s) seems to be more efficient at enhancing the selective anticancer cytoxicity of DCA than its UiO-66 analogue (SI, Figure S71).

Immune System Compatibility. In order to understand the possible effect of the MOFs towards cells of the immune system, such as macrophages and lymphocytes, the cell proliferation of J774 mouse macrophage cells and peripheral blood lymphocytes (PBLs) isolated from the blood of three human donors were investigated upon incubation with DCA-containing and empty MOFs (SI, Section S3). Both the empty and the DCA-containing MOFs were non-cytotoxic (cell proliferation >90%) after incubation with 0.5 mgmL^{-1} of MOF for both J774 cells (Figure 7c) and PBLs (Figure 7d). The reactive oxygen species (ROS) production in macrophages induced upon incubation with MOFs is represented in Figure 8a. Incubation with DCA@Zr-fum (s) induced the highest increase in ROS production (~3-fold) followed by DCA@Zr-fum-FA (CM) (~2.5-fold) and their empty analogues (~1.5-fold), while incubation with the PEGylated samples did not induce ROS production compared to the untreated control, even if it was the most internalised MOF.

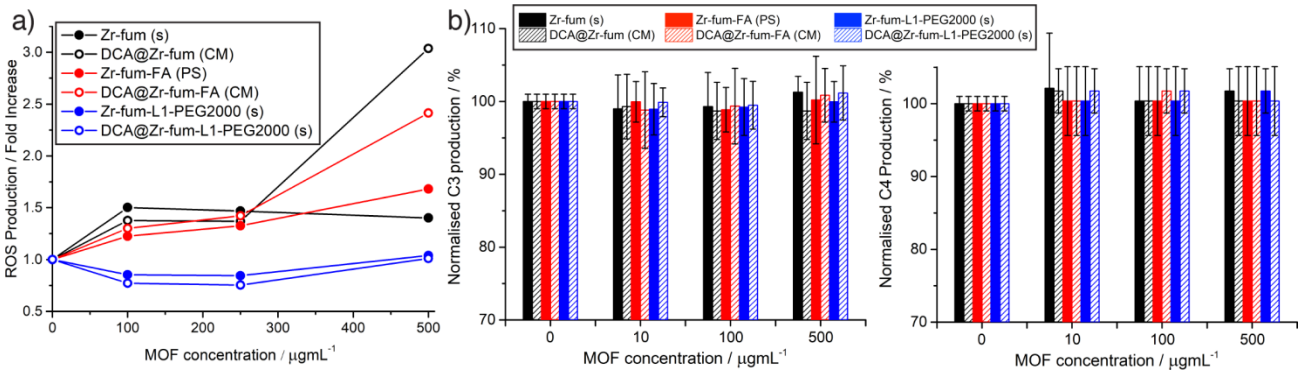

Figure 8. a) Reactive oxygen species (ROS) generation in J774 macrophage cells on exposure to empty and DCA-loaded Zr-fum samples. Complement cascade activation in human blood plasma induced by incubation with empty and DCA-loaded Zr-fum samples, plotted for production of b) C3 and c) C4 complement components, averaged from blood samples from three human donors.

The complement cascade activation (C3 and C4) was investigated upon incubation of blood plasma from three human donors with the MOFs. The complement cascade is a part of the immune system which eliminates foreign pathogens, and its activation usually results in activation of phagocytic cells and inflammation.[81] In Figures 8b and 8c, the data are represented as averages of the C3 and C4 concentrations, respectively, in serum of three different donors after treatment with different concentrations of the MOFs, normalised to a control in which blood plasma was treated with PBS. Individual data for each donor are given in the supporting information (Section S8), together with the hemolysis index upon treatment with each material. There was no significant difference from the control with PBS in any of the cases, meaning that the MOFs do not activate the complement cascade and so should be able to circulate in the blood without activation of phagocytes.

Conclusions

In the context of nanoscale drug delivery, the UiO series MOF linked by the endogeneous fumarate ligand, Zr-fum, has been shown to be amenable to size-controlled synthesis and surface modification by a number of protocols. The anticancer probe molecule DCA has been introduced to Zr-fum as a modulator during synthesis, with payloads of 20% *w/w* stored at defect sites, and the samples could also be surface modified without major DCA leakage. Cellular internalisation of Zr-fum was found to be size dependent; the smaller sample, Zr-fum (s) (~23 nm) was significantly better internalised by HeLa cervical cancer cells compared to the bigger analogue Zr-fum (b) (~170 nm), yet the latter was more internalised by macrophages, suggesting liver and spleen accumulation could be reduced by effective size refinement through *in vitro* studies previous to *in vivo* trials. Additionally, the efficient internalisation of the smaller MOFs at 4 ºC indicates that passive diffusion could play an important role in cellular uptake. While PEGylation of Zr-fum can induce caveolae-mediated endocytosis, as has been found to be the case for UiO-66,[29] folate coating in contrast does not result in caveolae-mediated uptake. PEGylation was proven to initially stabilise the MOFs towards phosphate attack on immersion in PBS, with an induction time with minimal degradation (< 5%) followed by similar degradation to the uncoated precursor MOF, possibly as a consequence of PEG corona cleavage. Additionally, postsynthetic surface modifications further improved the colloidal dispersion of the MOFs.

Use of the endogenous fumarate linker was expected to enhance biocompatibility of the MOFs compared to UiO-66 and other derivatives. The MOFs (both empty and DCA-loaded) were non-toxic towards a series of non-cancerous cell lines, including J774 macrophages, HEK293 kidney cells and lymphocytes isolated from the blood of human donors; some residual cytotoxicity of DCA@Zr-fum-L1-PEG2000 (s) towards kidney cells at high concentrations was the only concern. Only the PEGylated DCA@Zr-fum-L1-PEG2000 (s) induced cytotoxicity towards HeLa cancer cells, stopping all proliferation when incubated at 0.5 $mgmL^{-1}$ (ca 0.06 $mgmL^{-1}$ DCA) indicating that internalisation through the caveolae-mediated route enhances the therapeutic effect of DCA by a factor of 200. All three DCA-containing samples were cytotoxic towards MCF-7 breast cancer cells, with the PEGylated MOF once again the most effective for delivery of DCA, and more effective for delivery of DCA than its UiO-66 analogue. The composition of Zr-fum was also expected to mediate immune system response, in addition to the small size decreasing macrophage uptake. Surface modification did not notably change uptake of the MOFs by macrophage cells and had no effect on proliferation, while both empty and DCA-containing Zr-fum-L1-PEG2000 (s) did not induce significant ROS production; the bare sample induced the highest ROS production, with a 3-fold increase, which is less than observed for related UiO-66

nanoparticles.[28] Complement cascades (C3 and C4) in the blood plasma of three different human donors were not activated upon incubation with any of the empty or DCA-loaded MOFs, again showing good toleration of the nanoparticles by important immune system species.

Taken together, the improvement in both selective *in vitro* anticancer cytotoxicity and immune system compatibility compared to UiO-66 suggest Zr-fum is an excellent candidate for further investigation as a drug delivery device, with fine control over particle size and functionality possible. Additionally, the study highlights the *in vitro* experimental toolkit available to allow tuning of a range of properties of DDSs without invoking animal studies.

Acknowledgements

R.S.F. and D.F.-J. thank the Royal Society for the receipt of University Research Fellowships. R.S.F. and I.A.L. thank the University of Glasgow for funding. This project received funding in part from the European Research Council (ERC) under the European Union's Horizon 2020 Programme for Research and Innovation (grant agreement no. 677289, SCoTMOF, ERC-2015-STG).

Supporting Information

Synthetic procedures, surface functionalization protocols, full experimental characterization of materials, drug-loading protocols, stability tests, cytotoxicity assays, and immune system response assays.

Notes

The authors declare no competing financial interest. The data which underpin this work are available at http://dx.doi.org/10.5525/gla.researchdata.656.

References

1. Partridge, A. H.; Burstein, H. J.; Winer, E. P., Side Effects of Chemotherapy and Combined Chemohormonal Therapy in Women With Early-Stage Breast Cancer. *J. Natl. Cancer Inst. Monogr.* **2001,** *2001*, 135-142.
2. Ramirez, L. Y.; Huestis, S. E.; Yi Yap, T.; Zyzanski, S.; Drotar, D.; Kodish, E., Potential Chemotherapy Side Effects: What Do Oncologists Tell Parents? *Pediatr. Blood Cancer* **2009,** *52*, 497-502.
3. Sun, C. C.; Bodurka, D. C.; Weaver, C. B.; Rasu, R.; Wolf, J. K.; Bevers, M. W.; Smith, J. A.; Wharton, J. T.; Rubenstein, E. B., Rankings and symptom assessments of side effects from chemotherapy: insights from experienced patients with ovarian cancer. *Support. Care Cancer* **2005,** *13*, 219-227.
4. Kim, K. Y., Nanotechnology platforms and physiological challenges for cancer therapeutics. *Nanomedicine* **2007,** *3*, 103-110.

5. Baeza, A.; Ruiz-Molina, D.; Vallet-Regí, M., Recent advances in porous nanoparticles for drug delivery in antitumoral applications: inorganic nanoparticles and nanoscale metal-organic frameworks. *Expert Opin. Drug Deliv.* **2017,** *14*, 783-796.
6. Sur, S.; Fries, A. C.; Kinzler, K. W.; Zhou, S.; Vogelstein, B., Remote loading of preencapsulated drugs into stealth liposomes. *Proc. Natl. Acad. Sci. USA* **2014,** *111*, 2283-2288.
7. Huang, X.; Brazel, C. S., On the importance and mechanisms of burst release in matrix-controlled drug delivery systems. *J. Control. Release* **2001,** *73*, 121-136.
8. Bellido, E.; Guillevic, M.; Hidalgo, T.; Santander-Ortega, M. J.; Serre, C.; Horcajada, P., Understanding the Colloidal Stability of the Mesoporous MIL-100(Fe) Nanoparticles in Physiological Media. *Langmuir* **2014,** *30*, 5911-5920.
9. Jarockyte, G.; Daugelaite, E.; Stasys, M.; Statkute, U.; Poderys, V.; Tseng, T.-C.; Hsu, S.-H.; Karabanovas, V.; Rotomskis, R., Accumulation and Toxicity of Superparamagnetic Iron Oxide Nanoparticles in Cells and Experimental Animals. *Int. J. Mol. Sci.* **2016,** *17*, 1193.
10. Yu, Y.; Li, Y.; Wang, W.; Jin, M.; Du, Z.; Li, Y.; Duan, J.; Yu, Y.; Sun, Z., Acute Toxicity of Amorphous Silica Nanoparticles in Intravenously Exposed ICR Mice. *PLoS One* **2013,** *8*, e61346.
11. Blanco, E.; Shen, H.; Ferrari, M., Principles of nanoparticle design for overcoming biological barriers to drug delivery. *Nat. Biotechnol.* **2015,** *33*, 941-951.
12. Yaghi, O. M.; Li, H., Hydrothermal Synthesis of a Metal-Organic Framework Containing Large Rectangular Channels. *J. Am. Chem. Soc.* **1995,** *117*, 10401-10402.
13. Moghadam, P. Z.; Li, A.; Wiggin, S. B.; Tao, A.; Maloney, A. G. P.; Wood, P. A.; Ward, S. C.; Fairen-Jimenez, D., Development of a Cambridge Structural Database Subset: A Collection of Metal–Organic Frameworks for Past, Present, and Future. *Chem. Mater.* **2017,** *29*, 2618-2625.
14. Saul, J. M.; Annapragada, A.; Natarajan, J. V.; Bellamkonda, R. V., Controlled targeting of liposomal doxorubicin via the folate receptor in vitro. *J. Control. Release* **2003,** *92*, 49-67.
15. Javadi, M.; Pitt, W. G.; Tracy, C. M.; Barrow, J. R.; Willardson, B. M.; Hartley, J. M.; Tsosie, N. H., Ultrasonic gene and drug delivery using eLiposomes. *J. Control. Release* **2013,** *167*, 92-100.
16. Lu, J.; Liong, M.; Li, Z.; Zink, J. I.; Tamanoi, F., Biocompatibility, Biodistribution, and Drug-Delivery Efficiency of Mesoporous Silica Nanoparticles for Cancer Therapy in Animals. *Small* **2010,** *6*, 1794-1805.
17. Yu, T.; Hubbard, D.; Ray, A.; Ghandehari, H., In Vivo Biodistribution and Pharmacokinetics of Silica Nanoparticles as a Function of Geometry, Porosity and Surface Characteristics. *J. Control. Release* **2012,** *163*, 46-54.
18. Horcajada, P.; Serre, C.; Vallet-Regí, M.; Sebban, M.; Taulelle, F.; Férey, G., Metal–Organic Frameworks as Efficient Materials for Drug Delivery. *Angew. Chem. Int. Ed.* **2006,** *45*, 5974-5978.
19. Wu, M.-X.; Yang, Y.-W., Metal–Organic Framework (MOF)-Based Drug/Cargo Delivery and Cancer Therapy. *Adv. Mater.* **2017,** *29*, 1606134.
20. Horcajada, P.; Gref, R.; Baati, T.; Allan, P. K.; Maurin, G.; Couvreur, P.; Férey, G.; Morris, R. E.; Serre, C., Metal–Organic Frameworks in Biomedicine. *Chem. Rev.* **2012,** *112*, 1232-1268.
21. DeCoste, J. B.; Peterson, G. W.; Jasuja, H.; Glover, T. G.; Huang, Y.-G.; Walton, K. S., Stability and degradation mechanisms of metal-organic frameworks containing the $Zr_6O_4(OH)_4$ secondary building unit. *J. Mater. Chem. A* **2013,** *1*, 5642-5650.
22. Feng, D.; Gu, Z.-Y.; Li, J.-R.; Jiang, H.-L.; Wei, Z.; Zhou, H.-C., Zirconium-Metalloporphyrin PCN-222: Mesoporous Metal–Organic Frameworks with Ultrahigh Stability as Biomimetic Catalysts. *Angew. Chem. Int. Ed.* **2012,** *51*, 10307-10310.
23. Zirconium and its compounds [MAK Value Documentation, 1999]. In *The MAK-Collection for Occupational Health and Safety*, Wiley-VCH Verlag GmbH & Co. KGaA: 2002.

24. Marshall, R. J.; Forgan, R. S., Postsynthetic Modification of Zirconium Metal-Organic Frameworks. *Eur. J. Inorg. Chem.* **2016,** *2016*, 4310-4331.
25. Cavka, J. H.; Jakobsen, S.; Olsbye, U.; Guillou, N.; Lamberti, C.; Bordiga, S.; Lillerud, K. P., A New Zirconium Inorganic Building Brick Forming Metal Organic Frameworks with Exceptional Stability. *J. Am. Chem. Soc.* **2008,** *130*, 13850-13851.
26. Orellana-Tavra, C.; Marshall, R. J.; Baxter, E. F.; Lazaro, I. A.; Tao, A.; Cheetham, A. K.; Forgan, R. S.; Fairen-Jimenez, D., Drug delivery and controlled release from biocompatible metal-organic frameworks using mechanical amorphization. *J. Mater. Chem. B* **2016,** *4*, 7697-7707.
27. Nagata, S.; Kokado, K.; Sada, K., Metal-organic framework tethering PNIPAM for ON-OFF controlled release in solution. *Chem. Commun.* **2015,** *51*, 8614-8617.
28. Abánades Lázaro, I.; Haddad, S.; Rodrigo-Muñoz, J. M.; Orellana-Tavra, C.; del Pozo, V.; Fairen-Jimenez, D.; Forgan, R. S., Mechanistic Investigation into the Selective Anticancer Cytotoxicity and Immune System Response of Surface-Functionalized, Dichloroacetate-Loaded, UiO-66 Nanoparticles. *ACS Appl. Mater. Interfaces* **2018,** *10*, 5255-5268.
29. Abánades Lázaro, I.; Haddad, S.; Sacca, S.; Orellana-Tavra, C.; Fairen-Jimenez, D.; Forgan, R. S., Selective Surface PEGylation of UiO-66 Nanoparticles for Enhanced Stability, Cell Uptake, and pH-Responsive Drug Delivery. *Chem* **2017,** *2*, 561-578.
30. Chen, W.-H.; Yu, X.; Cecconello, A.; Yang Sung, S.; Nechushtai, R.; Willner, I., Stimuli-Responsive Nucleic Acid-Functionalized Metal-Organic-Framework Nanoparticles Using pH- and Metal-Ion Dependent DNAzymes as Locks. *Chem. Sci.* **2017,** *8*, 5769-5780.
31. Morris, W.; Briley, W. E.; Auyeung, E.; Cabezas, M. D.; Mirkin, C. A., Nucleic Acid–Metal Organic Framework (MOF) Nanoparticle Conjugates. *J. Am. Chem. Soc.* **2014,** *136*, 7261-7264.
32. He, C.; Lu, K.; Liu, D.; Lin, W., Nanoscale Metal–Organic Frameworks for the Co-Delivery of Cisplatin and Pooled siRNAs to Enhance Therapeutic Efficacy in Drug-Resistant Ovarian Cancer Cells. *J. Am. Chem. Soc.* **2014,** *136*, 5181-5184.
33. Yang, J.; Chen, X.; Li, Y.; Zhuang, Q.; Liu, P.; Gu, J., Zr-Based MOFs Shielded with Phospholipid Bilayers: Improved Biostability and Cell Uptake for Biological Applications. *Chem. Mater.* **2017,** *29*, 4580-4589.
34. Wang, S.; Morris, W.; Liu, Y.; McGuirk, C. M.; Zhou, Y.; Hupp, J. T.; Farha, O. K.; Mirkin, C. A., Surface-Specific Functionalization of Nanoscale Metal–Organic Frameworks. *Angew. Chem. Int. Ed.* **2015,** *54*, 14738–14742.
35. Chen, D.; Yang, D.; Dougherty, C. A.; Lu, W.; Wu, H.; He, X.; Cai, T.; Van Dort, M. E.; Ross, B. D.; Hong, H., In Vivo Targeting and Positron Emission Tomography Imaging of Tumor with Intrinsically Radioactive Metal–Organic Frameworks Nanomaterials. *ACS Nano* **2017,** *11*, 4315-4327.
36. Rocca, J. D.; Liu, D.; Lin, W., Nanoscale Metal–Organic Frameworks for Biomedical Imaging and Drug Delivery. *Acc. Chem. Res.* **2011,** *44*, 957-968.
37. Röder, R.; Preiß, T.; Hirschle, P.; Steinborn, B.; Zimpel, A.; Höhn, M.; Rädler, J. O.; Bein, T.; Wagner, E.; Wuttke, S.; Lächelt, U., Multifunctional Nanoparticles by Coordinative Self-Assembly of His-Tagged Units with Metal–Organic Frameworks. *J. Am. Chem. Soc.* **2017,** *139*, 2359-2368.
38. Wißmann, G.; Schaate, A.; Lilienthal, S.; Bremer, I.; Schneider, A. M.; Behrens, P., Modulated synthesis of Zr-fumarate MOF. *Micropor. Mesopor. Mater.* **2012,** *152*, 64-70.
39. Zahn, G.; Schulze, H. A.; Lippke, J.; König, S.; Sazama, U.; Fröba, M.; Behrens, P., A water-born Zr-based porous coordination polymer: Modulated synthesis of Zr-fumarate MOF. *Micropor. Mesopor. Mater.* **2015,** *203*, 186-194.
40. Furukawa, H.; Gándara, F.; Zhang, Y.-B.; Jiang, J.; Queen, W. L.; Hudson, M. R.; Yaghi, O. M., Water Adsorption in Porous Metal–Organic Frameworks and Related Materials. *J. Am. Chem. Soc.* **2014,** *136*, 4369-4381.
41. Kim, H.; Yang, S.; Rao, S. R.; Narayanan, S.; Kapustin, E. A.; Furukawa, H.; Umans, A. S.; Yaghi, O. M.; Wang, E. N., Water harvesting from air with metal-organic frameworks powered by natural sunlight. *Science* **2017,** *356*, 430-434.

42. Na, K.; Choi, K. M.; Yaghi, O. M.; Somorjai, G. A., Metal Nanocrystals Embedded in Single Nanocrystals of MOFs Give Unusual Selectivity as Heterogeneous Catalysts. *Nano Lett.* **2014,** *14*, 5979-5983.
43. Zhu, X.-H.; Yang, C.-X.; Yan, X.-P., Metal-organic framework-801 for efficient removal of fluoride from water. *Micropor. Mesopor. Mater.* **2018,** *259*, 163-170.
44. Ryu, U.; Yoo, J.; Kwon, W.; Choi, K. M., Tailoring Nanocrystalline Metal–Organic Frameworks as Fluorescent Dye Carriers for Bioimaging. *Inorg. Chem.* **2017,** *56*, 12859-12865.
45. Hermes, S.; Witte, T.; Hikov, T.; Zacher, D.; Bahnmüller, S.; Langstein, G.; Huber, K.; Fischer, R. A., Trapping Metal-Organic Framework Nanocrystals: An in-Situ Time-Resolved Light Scattering Study on the Crystal Growth of MOF-5 in Solution. *J. Am. Chem. Soc.* **2007,** *129*, 5324-5325.
46. Wang, S.; McGuirk, C. M.; d'Aquino, A.; Mason Jarad, A.; Mirkin Chad, A., Metal–Organic Framework Nanoparticles. *Adv. Mater.* **2018,** DOI: 10.1002/adma.201800202.
47. McGuire, C. V.; Forgan, R. S., The surface chemistry of metal-organic frameworks. *Chem. Commun.* **2015,** *51*, 5199-5217.
48. Shearer, G. C.; Chavan, S.; Bordiga, S.; Svelle, S.; Olsbye, U.; Lillerud, K. P., Defect Engineering: Tuning the Porosity and Composition of the Metal–Organic Framework UiO-66 via Modulated Synthesis. *Chem. Mater.* **2016,** *28*, 3749-3761.
49. Abanades Lazaro, I.; Abanades Lazaro, S.; Forgan, R. S., Enhancing anticancer cytotoxicity through bimodal drug delivery from ultrasmall Zr MOF nanoparticles. *Chem. Commun.* **2018,** *54*, 2792-2795.
50. Marshall, R. J.; Hobday, C. L.; Murphie, C. F.; Griffin, S. L.; Morrison, C. A.; Moggach, S. A.; Forgan, R. S., Amino acids as highly efficient modulators for single crystals of zirconium and hafnium metal-organic frameworks. *J. Mater. Chem. A* **2016,** *4*, 6955-6963.
51. Stefano, D.; Konstantin, E.; R., H. W.; Gregor, K.; Fischer. R. A., Defective Metal-Organic Frameworks. *Adv. Mater.* **2018**, DOI: 10.1002/adma.201704501.
52. Chithrani, B. D.; Ghazani, A. A.; Chan, W. C. W., Determining the Size and Shape Dependence of Gold Nanoparticle Uptake into Mammalian Cells. *Nano Lett.* **2006,** *6*, 662-668.
53. Treuel, L.; Jiang, X.; Nienhaus, G. U., New views on cellular uptake and trafficking of manufactured nanoparticles. *J. Royal Soc. Interface* **2013,** *10*, 20120939.
54. Orellana-Tavra, C.; Mercado, S. A.; Fairen-Jimenez, D., Endocytosis Mechanism of Nano Metal-Organic Frameworks for Drug Delivery. *Adv. Healthc. Mater.* **2016,** *5*, 2261-2270.
55. Rejman, J.; Oberle, V.; Zuhorn, I. S.; Hoekstra, D., Size-dependent internalization of particles via the pathways of clathrin- and caveolae-mediated endocytosis. *Biochem. J.* **2004,** *377*, 159-169.
56. Lim, J. P.; Gleeson, P. A., Macropinocytosis: an endocytic pathway for internalising large gulps. *Immunol. Cell Biol.* **2011,** *89*, 836-843.
57. Kiss, A. L.; Botos, E., Endocytosis via caveolae: alternative pathway with distinct cellular compartments to avoid lysosomal degradation? *J. Cell. Mol. Med.* **2009,** *13*, 1228-1237.
58. Taylor, P. R.; Martinez-Pomares, L.; Stacey, M.; Lin, H. H.; Brown, G. D.; Gordon, S., Macrophage receptors and immune recognition. *Annu. Rev. Immunol.* **2005,** *23*, 901-944.
59. Maherani, B.; Arab-Tehrany, E.; Kheirolomoom, A.; Geny, D.; Linder, M., Calcein release behavior from liposomal bilayer; influence of physicochemical/mechanical/structural properties of lipids. *Biochimie* **2013,** *95*, 2018-2033.
60. Orellana-Tavra, C.; Baxter, E. F.; Tian, T.; Bennett, T. D.; Slater, N. K. H.; Cheetham, A. K.; Fairen-Jimenez, D., Amorphous metal-organic frameworks for drug delivery. *Chem. Commun.* **2015,** *51* (73), 13878-13881.
61. Orellana-Tavra, C.; Haddad, S.; Marshall, R. J.; Abánades Lázaro, I.; Boix, G.; Imaz, I.; Maspoch, D.; Forgan, R. S.; Fairen-Jimenez, D., Tuning the endocytosis mechanism of Zr-based MOFs through linker functionalization. *ACS Appl. Mater. Interfaces* **2017,** *9*, 35516-35525.

62. Canton, I.; Battaglia, G., Endocytosis at the nanoscale. *Chem. Soc. Rev.* **2012,** *41*, 2718-2739.
63. Iversen, T.-G.; Skotland, T.; Sandvig, K., Endocytosis and intracellular transport of nanoparticles: Present knowledge and need for future studies. *Nano Today* **2011,** *6*, 176-185.
64. Sudimack, J.; Lee, R. J., Targeted drug delivery via the folate receptor. *Adv. Drug Deliv. Rev.* **2000,** *41*, 147-162.
65. Xie, J.; Xu, C.; Kohler, N.; Hou, Y.; Sun, S., Controlled PEGylation of Monodisperse Fe_3O_4 Nanoparticles for Reduced Non-Specific Uptake by Macrophage Cells. *Adv. Mater.* **2007,** *19*, 3163-3166.
66. Zwicke, G. L.; Mansoori, G. A.; Jeffery, C. J., Utilizing the folate receptor for active targeting of cancer nanotherapeutics. *Nano Rev.* **2012,** *3*, 18496.
67. Bannunah, A. M.; Vllasaliu, D.; Lord, J.; Stolnik, S., Mechanisms of Nanoparticle Internalization and Transport Across an Intestinal Epithelial Cell Model: Effect of Size and Surface Charge. *Mol. Pharm.* **2014,** *11*, 4363-4373.
68. Stacpoole, P. W., The pharmacology of dichloroacetate. *Metabolism* **1989,** *38*, 1124-1144.
69. Heshe, D.; Hoogestraat, S.; Brauckmann, C.; Karst, U.; Boos, J.; Lanvers-Kaminsky, C., Dichloroacetate metabolically targeted therapy defeats cytotoxicity of standard anticancer drugs. *Cancer Chemother. Pharmacol.* **2011,** *67*, 647-655.
70. Michelakis, E. D.; Webster, L.; Mackey, J. R., Dichloroacetate (DCA) as a potential metabolic-targeting therapy for cancer. *Br. J. Cancer* **2008,** *99*, 989-994.
71. Trapella, C.; Voltan, R.; Melloni, E.; Tisato, V.; Celeghini, C.; Bianco, S.; Fantinati, A.; Salvadori, S.; Guerrini, R.; Secchiero, P.; Zauli, G., Design, Synthesis, and Biological Characterization of Novel Mitochondria Targeted Dichloroacetate-Loaded Compounds with Antileukemic Activity. *J. Med. Chem.* **2016,** *59*, 147-156.
72. Stacpoole, P. W.; Nagaraja, N. V.; Hutson, A. D., Efficacy of dichloroacetate as a lactate-lowering drug. *J. Clin. Pharmacol.* **2003,** *43*, 683-691.
73. Zajac, J.; Kostrhunova, H.; Novohradsky, V.; Vrana, O.; Raveendran, R.; Gibson, D.; Kasparkova, J.; Brabec, V., Potentiation of mitochondrial dysfunction in tumor cells by conjugates of metabolic modulator dichloroacetate with a Pt(IV) derivative of oxaliplatin. *J. Inorg. Biochem.* **2016,** *156*, 89-97.
74. Mader, R. M.; Müller, M.; Steger, G. G., Resistance to 5-Fluorouracil. *Gen. Pharmac. Vasc. S.* **1998,** *31*, 661-666.
75. Tong, J.; Xie, G.; He, J.; Li, J.; Pan, F.; Liang, H., Synergistic Antitumor Effect of Dichloroacetate in Combination with 5-Fluorouracil in Colorectal Cancer. *J. Biomed. Biotechnol.* **2011,** *2011*, 740564.
76. Xuan, Y.; Hur, H.; Ham, I.-H.; Yun, J.; Lee, J.-Y.; Shim, W.; Kim, Y. B.; Lee, G.; Han, S.-U.; Cho, Y. K., Dichloroacetate attenuates hypoxia-induced resistance to 5-fluorouracil in gastric cancer through the regulation of glucose metabolism. *Exp. Cell Res.* **2014,** *321*, 219-230.
77. Khan, A.; Andrews, D.; Shainhouse, J.; Blackburn, A. C., Long-term stabilization of metastatic melanoma with sodium dichloroacetate. *World J. Clin. Oncol.* **2017,** *8*, 371-377.
78. Michelakis, E. D.; Sutendra, G.; Dromparis, P.; Webster, L.; Haromy, A.; Niven, E.; Maguire, C.; Gammer, T. L.; Mackey, J. R.; Fulton, D.; Abdulkarim, B.; McMurtry, M. S.; Petruk, K. C., Metabolic modulation of glioblastoma with dichloroacetate. *Sci. Transl. Med.* **2010,** *2*, 31ra34.
79. Stacpoole, P. W.; Gilbert, L. R.; Neiberger, R. E.; Carney, P. R.; Valenstein, E.; Theriaque, D. W.; Shuster, J. J., Evaluation of Long-term Treatment of Children With Congenital Lactic Acidosis With Dichloroacetate. *Pediatrics* **2008,** *121*, e1223-e1228.
80. Wong, J. Y.; Huggins, G. S.; Debidda, M.; Munshi, N. C.; De Vivo, I., Dichloroacetate induces apoptosis in endometrial cancer cells. *Gynecol. Oncol.* **2008,** *109*, 394-402.
81. Dobrovolskaia, M. A.; McNeil, S. E., Immunological properties of engineered nanomaterials. *Nat. Nanotechnol.* **2007,** *2*, 469-478.